

# Tuning Fano resonances by magnetic forces for electron transport through a quantum wire side-coupled to a quantum ring

B. Szafran and M.R. Poniedzialek

*Faculty of Physics and Applied Computer Science,*

*AGH University of Science and Technology, al. Mickiewicza 30, 30-059 Kraków, Poland*

(Dated: November 25, 2018)

We consider electron transport in a quantum wire with a side-coupled quantum ring in a two-dimensional model that accounts for a finite width of the channels. We use the finite difference technique to solve the scattering problem as well as to determine the ring-localized states of the energy continuum. The backscattering probability exhibits Fano peaks for magnetic fields for which a ring-localized states appear at the Fermi level. We find that the width of the Fano resonances changes at high magnetic field. The width is increased (decreased) for resonant states with current circulation that produce the magnetic dipole moment that is parallel (antiparallel) to the external magnetic field. We indicate that the opposite behavior of Fano resonances due to localized states with clockwise and counterclockwise currents results from the magnetic forces which change the strength of their coupling to the channel and modify the lifetime of localized states.

PACS numbers: 73.63.-b, 73.63.Nm, 73.63.Kv

## I. INTRODUCTION

Coherent transport properties of mesoscopic and nanoscale conductors is determined by interference conditions for the electron wave function at the Fermi level. Quantum dots and rings that are attached by a single contact to a conducting channel modify its magnetotransport properties although they lie outside the classical current path.<sup>1</sup> Single subband conductance of the contact is proportional to the electron transfer probability<sup>2</sup> and the latter is particularly sensitive to existence of localized states in the side-coupled structures. The localized states that belong to the energy continuum interfere with delocalized states of the channel leading to an appearance of Fano resonances<sup>3</sup> in magnetoconductance when the Fermi level of the channel is degenerate with the localized energy level. The Fano resonances for quantum dots and rings connected to a semiconducting channel by one or two contacts are extensively studied in the context of phase coherence probes,<sup>4</sup> Aharonov-Bohm interferometry,<sup>5</sup> Kondo effect,<sup>6-9</sup> construction of spin filters,<sup>10,11</sup> conductance of single-electron transistors,<sup>12</sup> arrays of quantum dots<sup>13-15</sup> and artificial defects.<sup>16,17</sup>

The transport properties of singly connected nanostructures are usually studied using theoretical models<sup>9-11,15-20</sup> that neglect the finite width of the channels. These models account for the phase shifts due to the Aharonov-Bohm effect but naturally overlook the deflection of electron trajectories by classical magnetic forces, which occurs when the Larmor radius is comparable to the width of the channel. The purpose of the present paper is to establish the role of magnetic deflection for the ballistic transport properties of a quantum ring side-coupled to a channel.

The magnetic forces were previously considered<sup>21,22</sup> for quantum rings that are embedded within the channel.<sup>23-27</sup> In these structures the Lorentz force leads to a preferential injection of the electron from the input

channel to one of the arms of the ring.<sup>21</sup> The preferential injection implies reduction of the Aharonov-Bohm interference amplitude at the exit to the output channel.<sup>21</sup> A theoretical study of a ring connected to three channels,<sup>22</sup> indicated that the reduction of the Aharonov-Bohm conductance oscillations due to magnetic forces is accompanied by a distinct imbalance of the electron transfer to the two output terminals. This prediction<sup>22</sup> was confirmed in a subsequent experiment.<sup>28</sup> In a recent proposal<sup>29,30</sup> of electronic interaction-free measurement, the idea for the solid state device employs magnetic forces to deflect the electron trajectory in a similar manner as beam splitters deflect the photons in the optical experimental setup,<sup>31</sup> which introduces an additional interest in magnetic forces.

In this paper we solve the single subband scattering problem for a quantum ring singly connected to a quantum wire in presence of perpendicular magnetic field. The resonances that are found in the electron backscattering probability are confronted with the results of the stabilization method<sup>32</sup> which allows for detection of localized states in the energy continuum. We find that injection of the electron from the channel to the ring is enhanced at the resonances. The charge distribution within the structure is not an even function of the magnetic field. This direct effect of magnetic forces does not influence the linear conductance which is necessarily an even function of the magnetic field due to the Onsager symmetry.<sup>33</sup> We demonstrate that for a finite width of the channel the Fano resonances of backscattering probability change in a characteristic manner at high magnetic field. Typically these resonances appear in pairs. We find that at high magnetic field one of the resonances widens, and the other becomes extremely thin. We argue that modification of the width of resonances is uniquely due to magnetic forces. Thermal stability of Fano resonances of backscattering probability is also discussed.

The Fano resonances in weak magnetic fields were con-

sidered in particular in Refs. 34 and 35 for quantum dots embedded within a channel. Ref. 35 describes the quantum-dot-localized states of the energy continuum between the first and second subband propagation thresholds that are of the odd parity symmetry with respect to the axis of the system. These states are bound, i.e. have an infinite lifetime, since the leakage to the channel is blocked by the opposite - even parity - symmetry of the lowest subband of the channel. The magnetic field breaks the symmetry with respect to the axis of the system and allows for the electron leakage. The bound states turn into metastable ones with a finite lifetime and the backscattering probability exhibits Fano peaks that shift on the energy scale with the magnetic field according to the sign of the dipole moment produced by the current circulation in the quantum-dot-localized states. The study<sup>35</sup> is limited to weak magnetic fields, and does not cover the modification of the lifetime due to magnetic forces which are the subject of the present paper.

This paper is organized as follows. In Section II we briefly describe the approach applied for the scattering problem. The stabilization method for localized states detection is sketched in Section III. The results of these two approaches are confronted in Section IV. Summary and conclusions are given in Section V.

## II. TREATMENT OF SCATTERING PROBLEM

The studied system is presented in Fig. 1. We assume that the channels are made of GaAs embedded in  $\text{Al}_{0.45}\text{Ga}_{0.55}\text{As}$  matrix. The width of the channels is taken equal to 64 nm, unless explicitly stated otherwise. The inner (outer) radius of the ring is 60 nm (124 nm). The electron confinement in the growth direction is usually much stronger than the planar one, which justifies application of a two-dimensional model that is employed below. We consider the Hamiltonian

$$H = (\mathbf{p} + e\mathbf{A}(\mathbf{r}))^2 / 2m^* + V(x, y) \quad (1)$$

where  $-e$  is the electron charge ( $e > 0$ ) and  $m^* = 0.067m_0$  is the GaAs electron band effective mass. We apply the Lorentz gauge  $\mathbf{A} = (A_x, A_y, 0) = (0, Bx, 0)$  and assume that the confinement potential  $V(x, y)$  is zero inside (the blue area in Fig. 1) and  $V_0 = 200$  meV<sup>36</sup> outside the channels (the white area in Fig. 1).

We solve the eigenequation

$$H\Psi = E\Psi \quad (2)$$

with a finite difference approach using a square grid and lattice spacings  $\Delta x = \Delta y = 2$  nm to determine the wave function on a mesh  $\Psi_{\mu, \nu} = \Psi(x_\mu, y_\nu)$ . In the calculation we use the gauge-invariant discretization of the kinetic energy operator<sup>39</sup>

$$\frac{1}{2m^*} (\mathbf{p} + e\mathbf{A}(\mathbf{r}))^2 \Psi_{\mu, \nu} = \frac{\hbar^2}{2m^* \Delta x^2} \times$$

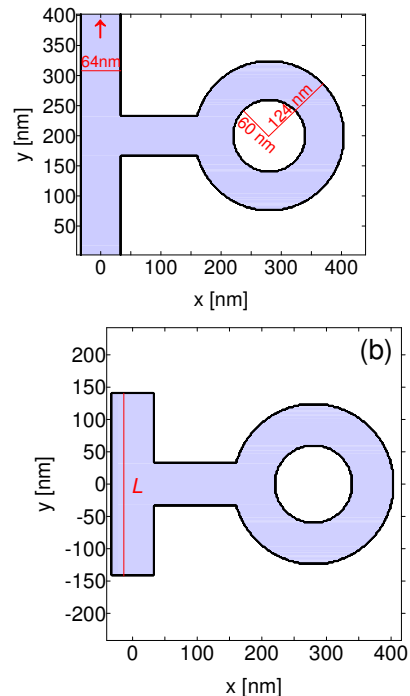


FIG. 1: (a) The system studied in the scattering problem. The electron is assumed to come from the channel below the contact to the ring and the vertical channel has an infinite length. (b) The model system used for determination of the ring-localized states.  $L$  is the finite length of the channel, which varies in the calculation. The confinement potential is assumed 0 within the blue area and 200 meV in the outside.

$$(4\Psi_{\mu, \nu} - C_y \Psi_{\mu, \nu-1} - C_y^* \Psi_{\mu, \nu+1} - \Psi_{\mu-1, \nu} - \Psi_{\mu+1, \nu}), \quad (3)$$

with  $C_y = \exp[-i\frac{e}{\hbar}\Delta x Bx]$ .

For description of electron scattering we assume that the input channel is the one below the contact to the ring [Fig. 1(a)]. For the chosen gauge the Hamiltonian eigenfunctions in the channel can be written in a separable form

$$\Psi(x, y) = \exp(iky)\psi^k(x), \quad (4)$$

where  $k$  is the wave vector and  $\psi^k(x)$  is the transverse eigenfunction of the electron in the vertical channel, which is determined by solution of a one-dimensional equation obtained by plugging Eq. (4) into the Schrodinger equation (2). For the energy that corresponds to the lowest subband the wave function in the incoming lead far from the ring is a superposition of the incident and reflected waves

$$\Psi = \psi^k(x) \exp(iky) + c_{-k} \psi^{-k}(x) \exp(-iky), \quad (5)$$

and far in the output lead one has only the transferred wave function

$$\Psi = d_k \psi^k(x) \exp(iky). \quad (6)$$

The values of  $c_{-k}$  and  $d_k$  are extracted from the finite difference wave functions at the ends of the computational box.

The boundary condition of the output lead (6) is introduced to the discretized eigenequation (2) in a Neumann form

$$\Psi_{\mu,\nu+1} = \Psi_{\mu,\nu} \exp(ik\Delta y) \quad (7)$$

that results of Eq. (6). The boundary condition for the input lead (5) is taken in the Dirichlet form with an initial assumption that  $c_{-k} = 0$ . After solution of the algebraic form of the eigenequation we extract  $c_{-k}$  and  $d_k$  by analyzing the finite difference wave function at the ends of the channels. The eigenequation is solved for the new value of  $c_{-k}$  introduced in the boundary condition. The procedure converges after just a few iterations.<sup>37</sup>

After the convergence is reached we evaluate the backscattering probability by calculating the current fluxes in the incoming channel

$$R = \frac{\int dx j^{-k}(x)}{\int dx j^k(x)}, \quad (8)$$

where  $j^k$  is the probability density current associated to the incoming part of the wave function of Eq. (5),

$$j^k(x) = \frac{\hbar}{m^*} |\psi^k(x)|^2 (\hbar k + eBx) \quad (9)$$

and  $j^{-k}$  corresponds to the backscattered one

$$j^{-k}(x) = \frac{\hbar}{m^*} |c_{-k}|^2 |\psi^{-k}(x)|^2 (-\hbar k + eBx). \quad (10)$$

The backscattering probability is related to magnetoconductance<sup>2</sup> as  $G(B) = \frac{2e^2}{h} [1 - R(B)]$ .

The magnetic forces modify the width of the Fano resonances of the backscattering probability not only as a function of the magnetic field but also as a function of the energy. In finite temperature a transport window is opened near the Fermi level  $E_F$  and the narrow Fano resonances are likely to be thermally unstable. The stability of Fano resonances against thermal excitations is below estimated by the linear response formula

$$\overline{R}(E_F) = \int R(E) \left( -\frac{\partial f}{\partial E} \right) dE, \quad (11)$$

where  $f$  is the Fermi function  $f = (e^{(E-E_F)/k_B T} + 1)^{-1}$ .  $T$  stands for the temperature and  $k_B$  for the Boltzmann constant.

### III. DETECTION OF LOCALIZED STATES

In order to determine the resonant states localized in the ring we use the stabilization method.<sup>32</sup> For this purpose we assume that the vertical channel has a finite length [see Fig. 1(b)]. Then we solve the eigenequation

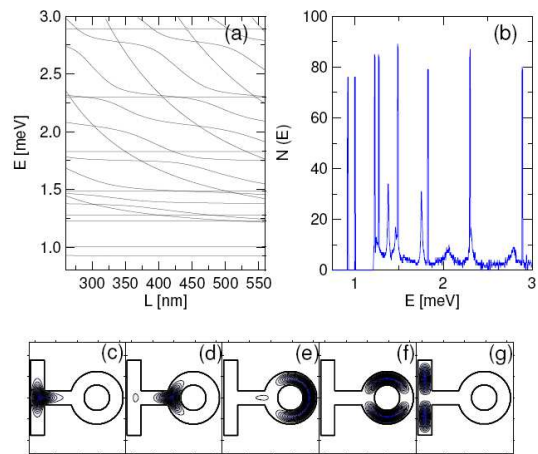


FIG. 2: (a) Energy spectrum for the channel of a finite length ( $L$ ) for  $B = 0$ . (b) The peaks indicate the energies of the localized states extracted of the energy spectrum according to Eq. (12). (c-e) Charge densities of the five lowest energy eigenstates for  $L = 352$  nm. Plot (c) corresponds to the ground-state, (d) to the first excited state etc.

(4) with boundary conditions that require the wave functions to vanish at all the edges of the computational box. We calculate the energy spectrum as a function of the length of the channel  $L$ . The energy spectrum that is discrete for finite  $L$  is displayed in Fig. 2(a) for  $B = 0$ . We see that some energy levels decrease as  $L$  grows. They correspond to electron states in the channel. The energy of states localized in the ring are independent of  $L$ .

The two lowest energy levels of Fig. 2(a) correspond to states localized at one of T-junctions<sup>38</sup> present in the system – one between the main vertical channel and the short horizontal one [Fig. 2(c)], and the other between the latter and the quantum ring [Fig. 2(d)]. These two states are not only localized but energetically bound – their energies (0.925 meV and 1.006 meV) lie below the continuum threshold. The threshold is determined by the bottom of the lowest subband ( $k = 0$ ) for the infinite vertical channel. For 64 nm - wide channel the energy continuum starts above 1.147 meV ( $B = 0$ ). The energy levels of Fig. 2(a) above the continuum threshold that are independent of  $L$  correspond to the ring-localized states, see Figs. 2(e) and 2(f). The fourth excited state [Fig. 2(g)] found for  $L = 352$  nm corresponds to the electron within the channel, and its energy distinctly depends on  $L$  [see Fig. 2(a) for  $L = 352$  nm].

The spectral positions of the localized states are determined by counting the states of the energy close to  $E$ ,

$$N(E) = \int dL \sum_l \delta(|E - E_l(E)|; dE), \quad (12)$$

where  $l$  numbers the Hamiltonian eigenvalues for the finite size of the system, and  $\delta(|E - E_l(L)|; dE)$  is equal

to 1 for  $|E - E_l(L)| < dE$  and 0 otherwise. In Fig. 2(b) we plotted  $N(E)$  calculated for the energy spectrum of Fig. 2(a) with the energy window  $dE = 5\mu\text{eV}$ .

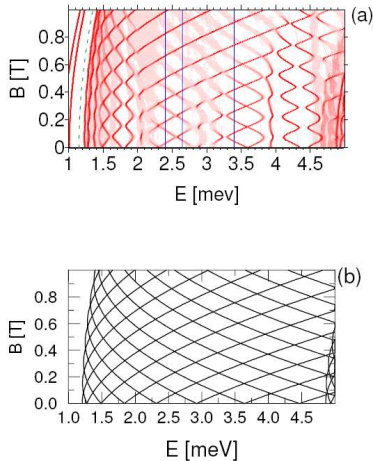


FIG. 3: (a) Positions of localized states in the energy continuum as calculated by formula (12). The darker the shade of red the larger value of  $N(E)$ . The thin vertical lines indicate energies of 2.4, 2.65 and 3.4 meV that are considered in detail below. The green dashed line indicates the continuum threshold (ground-state energy of the electron within the channel for  $k = 0$ ). (b) Energy spectrum of the closed circular quantum ring that is not connected to the channel.

Figure 3 shows how the maxima of  $N(E)$  shift with  $B$  [Fig. 3(a)] as compared to the energy spectrum of a closed<sup>40</sup> quantum ring [Fig. 3(b)] that is not connected to the channel. The two lowest-energy lines of Fig. 3(a) correspond to states localized at the junctions. The resonances that are higher in the energy correspond to states localized in the ring. The positions of resonances oscillate with magnetic field with a period of 0.165 T that results from the Aharonov-Bohm effect for a ring of an effective radius of 92 nm. The resonances enter into avoided crossings that result from angular momentum mixing of closed-ring states. The mixing is due to the presence of the contact that breaks the rotational symmetry and is the strongest at odd multiples of half of the flux quantum threading the ring. Above 4.6 meV the states of the second subband - with wave functions that change sign across the channel appear in Fig. 3(a). For the closed ring these states appear near 4.9 meV [Fig. 3(b)].

#### IV. RESONANCES IN THE QUANTUM RESISTANCE

Now let us look at the electron backscattering probability that is plotted with the black line in Fig. 4(a) for  $E = 2.65$  meV. The red lines in Fig. 4(a) show the resonance detection counter  $N(E)$  of Eq. (12).  $R$  exhibits peaks as a function of the magnetic field. These peaks perfectly coincide on the magnetic field scale with

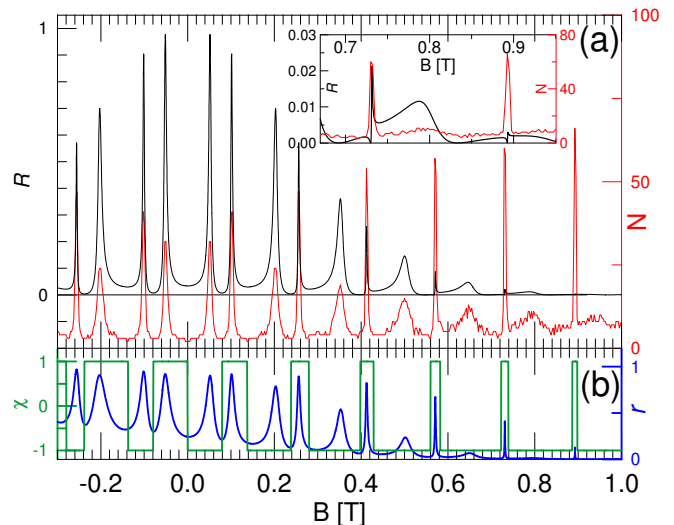


FIG. 4: (a) Black line shows the electron backscattering probability for energy  $E = 2.65$  meV and the red one - the value of the resonance detection counter  $N(E)$  [Eq.(12)]. The inset shows a zoom of high  $B$  part of the figure. (b) The value of  $\chi$  plotted in green indicates the direction of the current circulation inside the ring:  $\chi = 1$  (-1) corresponds to counterclockwise (clockwise) direction. The blue line shows the fraction of the probability density  $r$  that is contained within the ring, i.e. for  $x > 32.5$  nm of the computational box of Fig. 1(a).

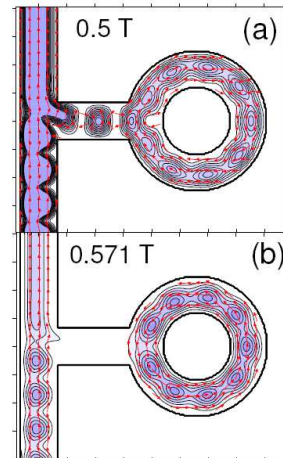


FIG. 5: The contours show the charge density for two peaks of backscattering probability of Fig. 4 obtained for  $E = 2.65$  meV at  $B = 0.5$  T (a) and at  $B = 0.751$  T (b). The arrows show the probability current distribution.

the positions of the ring-localized states as determined by the stabilization method. The backscattering occurs only when the channel state carrying the current is degenerate with a localized state within the ring. Outside the degeneracy the structure is nearly transparent for the electron transfer. The peaks of  $R$  have distinctly asymmetric

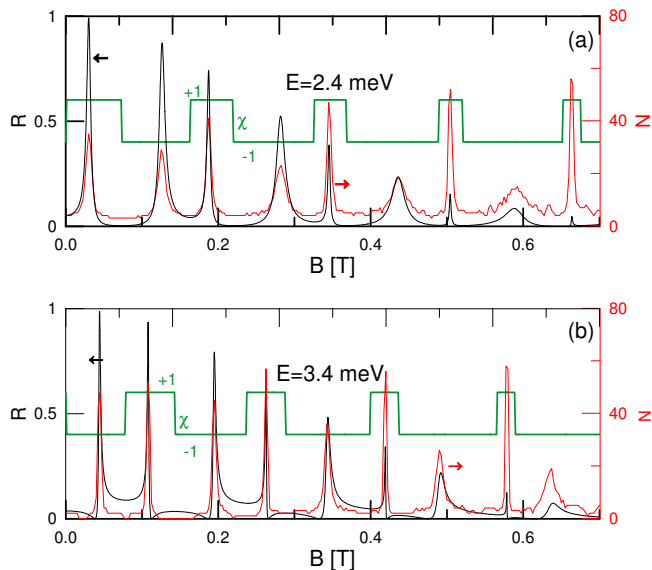


FIG. 6: Backscattering probability (black line, left axis), the resonance counter [Eq.(12), red line, right axis] and the direction of the current circulation within the ring in the scattering eigenstates [green line,  $\chi = +1$  ( $-1$ ) corresponds to counterclockwise (clockwise) orientation]. Plots (a) and (b) were prepared for  $E = 2.4$  meV and  $3.4$  meV, respectively.

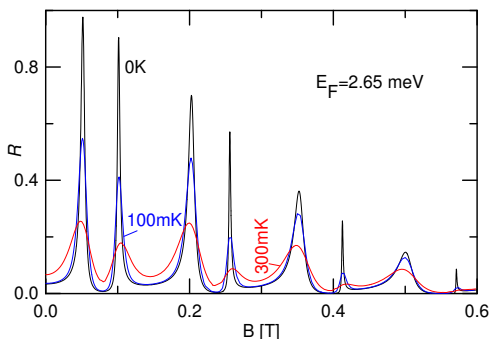


FIG. 7: The backscattering probability averaged according to the linear response formula (11) for the Fermi energy assumed at  $2.65$  meV for  $0$  K (black line),  $100$  mK (blue line) and  $300$  mK (red line).

shape which is a characteristic signature of a resonance involving a localized state of the energy continuum.<sup>3</sup>

In Fig. 4(b) we plotted with the blue line the fraction  $r$  of the probability density stored by the computational box of Fig. 1(a) that is contained within the ring (outside the vertical channel in fact). We notice that the electron enters the ring for magnetic fields for which a localized state is present at the considered energy. Note that  $R$  is an even function of  $B$  but  $r$  is not [ $r(B) \neq r(-B)$ ]. For  $B > 0$  the Lorentz force deflects the electron trajectories to the left of its momentum vector, hence the penetration of the wave function to the ring is hampered for positive and enhanced for negative magnetic field.

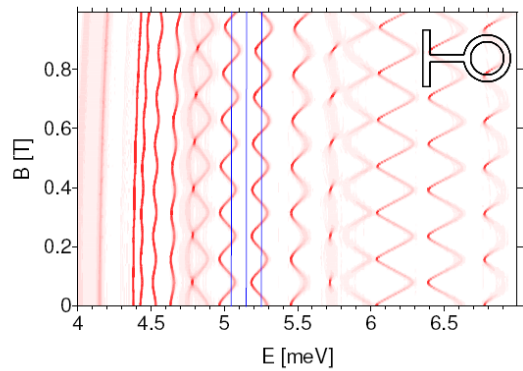


FIG. 8: Same as Fig. 4(a) but for the channel width reduced to  $32$  nm. The inner and outer radii of the side-coupled ring are  $76$  and  $108$  nm, respectively. The geometry is displayed in the inset. The thin vertical lines indicate energies of  $5.05$ ,  $5.16$  and  $5.26$  meV that are considered in Fig. 9.

The height of  $R$  maxima is reduced for high magnetic field. For  $B > 0$  the Lorentz force pushes the electron to the left edge of the vertical channel. The electron with wave function shifted to the left edge of the channel seems not to notice the presence of the ring and passes through the contact with a nearly  $100\%$  probability. At high  $B$  the presence of the ring still produces the Fano peaks but on a tiny scale [see the inset to Fig. 4(a)]. In this sense the Lorentz force for  $B > 0$  assists in the electron transport across the contact. Note, that due to the microreversibility relation<sup>33</sup> we have  $R(B) = R(-B)$  although for negative  $B$  the electron penetration to the ring is enhanced.

The results for  $N(E)$  as presented in Fig. 4(a) are cross section of Fig. 3(a) taken along the constant energy line. We can see that the line for  $E = 2.65$  meV crosses the resonances of Fig. 3(a) that grow or decrease in energy as the magnetic field grows. The magnetic dipole moment generated by currents is  $\mu = -\frac{dE}{dB}$ . For a strictly one dimensional closed circular quantum ring  $\mu = -\frac{1}{2}\mathbf{er} \times \mathbf{j}$ , where  $\mathbf{j}$  stands for the probability density current. Thus, the resonances that grow (decrease) in the energy correspond to localized states in which the current circulates counterclockwise (clockwise) around the ring and produce magnetic dipole moment that is antiparallel (parallel) to the external magnetic field. The direction of the current flow within the ring as found in the solution of the scattering problem is denoted by  $\chi = \pm 1$  [green line in Fig. 4(b)], where the plus sign stands for the counterclockwise circulation. Note, that  $\chi$  changes sign between each minimum of the transfer probability. For  $B > 0$  the resonances that increase (decrease) in width corresponds to clockwise (counterclockwise) current circulation. At high positive magnetic field the current circulation within the ring in the scattering eigenstates is counterclockwise with the exception of  $B$  ranges that surround the sharp Fano resonances [Fig. 4(b)].

Figure 5 shows the charge density and current distri-

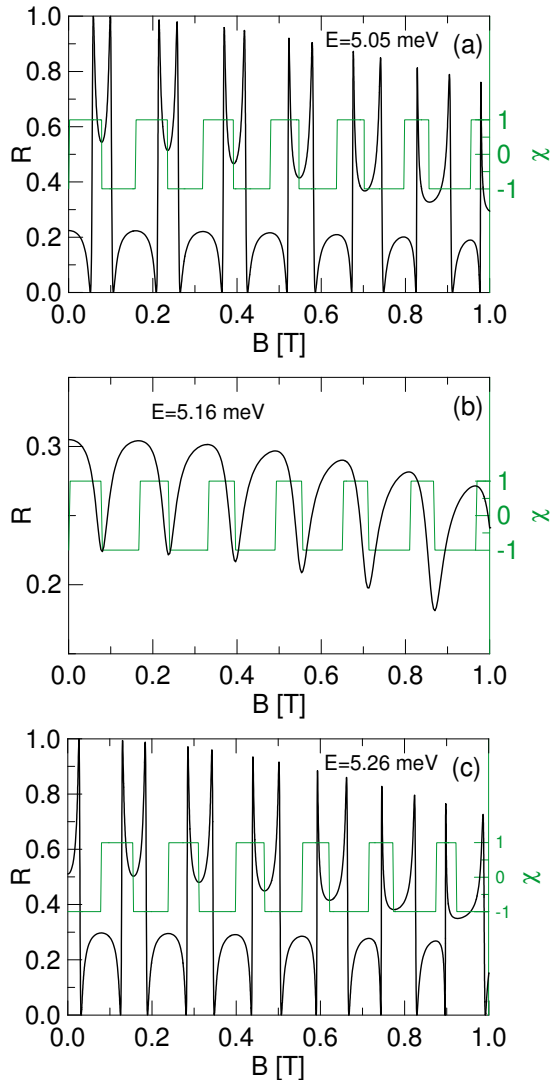


FIG. 9: Backscattering probability (black line, left axis), and the direction of the current circulation within the ring in the scattering eigenstates [green line,  $\chi = +1$  (-1) corresponds to counterclockwise (clockwise) orientation]. Plots (a,b,c) were prepared for  $E = 5.05$ ,  $5.16$  and  $5.26$  meV, for the structure parameters of Fig. 8.

tribution for two backscattering peaks of Fig. 4(a), a wide one [Fig. 5(a)] and a narrow one [Fig. 5(b)]. In both these cases the charge density is pushed to the left with respect to the electron "velocity", i.e. to the external edge of the ring for the wide peak [Fig. 5(a)] and to the internal edge of the ring for the narrow one [Fig. 5(b)]. The clockwise orientation of the current circulation is at high magnetic field translated by the Lorentz force into stronger coupling of the localized states to the conducting channel [Fig. 5(a)]. The electron of the ring-localized state is "ejected" into the horizontal link to the main channel by the Lorentz force. The charge density within the horizontal channel acquires similar values to the ones within the ring. The stronger coupling for these

states leads to an increased width of the resonance, or in other words to a decreased lifetime of the ring localized state. Opposite effects are observed for resonances with localized states of counterclockwise current circulation, for which the Lorentz force tends to keep the electron within the ring, increases the localized state lifetime and thus reduces the width of the resonance in the transfer probability.

Let us count the resonances for positive  $B$  starting from zero field, for the energies marked by thin blue lines in Fig. 3(a). For  $E = 2.65$  meV – the case that was discussed above – the Fano resonances that become narrow at high  $B$  correspond to *even* resonance numbers. For  $E = 2.4$  meV the first resonance is obtained for a localized state with a counterclockwise current circulation that grows in the energy for increasing  $B$  [Fig. 3(a)]. Accordingly, Fig. 6(a) shows that the resonances that become narrow at high  $B$  correspond to *odd* resonance numbers [see Fig. 3(a)]. For  $E = 3.4$  meV [Fig. 9(b)] the odd (even) peaks increase (decrease) in width as for  $E = 2.65$  meV in consistence with the order of resonances crossed at this energy in function of  $B$  of Fig. 3(a).

Fig. 7 shows the backscattering probability averaged over the transport window opened near the Fermi energy assumed equal  $2.65$  meV for  $T = 100$  mK and  $300$  mK according to Eq.(11). The resonances that corresponds to ring localized states with counterclockwise current circulation are less thermally stable than the ones with the clockwise flowing current.

For completeness we present results for the structure that is closer to the one-dimensional limit. For this purpose we reduce the channel width from  $64$  to  $32$  nm. The shape of the ring with thin channels is displayed in the inset to Fig. 8. We keep the axis of the vertical channel as well as the center of the ring in unchanged positions, and set the outer and inner radii of the ring equal to  $108$  and  $76$  nm, respectively to maintain the same Aharonov-Bohm period as in the structure considered above.

Fig. 8 shows the positions of localized states as determined by the stabilization method. The stronger transverse confinement increases significantly the energy of the low part of the spectrum and enlarges the avoided crossing due to the presence of the contact. The vertical lines in Fig. 8 indicate the energies for which we display also the  $0\text{K}$  backscattering probability:  $5.05$  meV [Fig. 9(a)],  $5.16$  meV [Fig. 9(b)] and  $5.26$  meV [Fig. 9(c)]. The energy of  $5.05$  meV lies within the wide gap opened by the avoided crossing of localized energy levels. The case presented in Fig. 9(b) corresponds to the energy for which no resonances are found in function of the magnetic field. The oscillations of  $R$  have a small amplitude and are due to the Aharonov-Bohm phase shifts within the ring. For the two other energies considered here, the Fano resonances are distinctly present in  $R(B)$  dependence [Fig. 9(a) and 9(c)]. The maxima of  $R$  are close to  $1$  and decrease in function of  $B$  more slowly than for the wide structure considered above [see Figs. 4 and 6], since the shift of the electron density within the channel due

to the Lorentz force is hampered by the much stronger confinement. The Fano resonances that become thin in both cases considered in Figs. 9(a) and 9(c) correspond to counterclockwise circulation of the current within the ring. Concluding, the modification of the width and height of resonances are of the same origin and form as for the wide channels, only the effects of magnetic forces are of a reduced strength. We also note that for the thin channels the backscattering probability is of the order of 0.25% outside the resonances as compared to nearly zero for the wider channels discussed above.

## V. SUMMARY AND CONCLUSION

We have studied the electron transport in a channel side-coupled to a quantum ring taking into account the finite width of the structure. The evaluated backscattering probability exhibits Fano peaks for magnetic fields for which the ring-localized states of the energy continuum

are degenerate with the Fermi level. We have demonstrated that the ring-localized states that correspond to current circulation producing a magnetic dipole moment that is antiparallel to the external magnetic field produce very thin Fano resonances. The localized states with the dipole moment that is aligned with the magnetic field vector result in resonances that become wider at high magnetic field. The latter are also more thermally stable. The opposite behavior of these two types of resonances is due to shifts of the radial wave function of ring-localized states induced by magnetic forces which increase or decrease the coupling to the channel depending on the direction of the current circulation. The described effect can be used to tune the Fano resonances for potential applications<sup>10,11,13</sup> or for magnetic forces detection.

**Acknowledgements** This work was performed within a research project N N202 103938 supported by Ministry of Science and Higher Education (MNiSW) for 2010-2013. Calculations were performed in ACK-CYFRO-NET-AGH on the RackServer Zeus.

- 
- <sup>1</sup> R.A. Webb and S. Washburn, *Phys. Today* **41**, 46 (1988).  
<sup>2</sup> M. Büttiker, *Phys. Rev. B* **38**, 9375 (1988).  
<sup>3</sup> U. Fano, *Phys. Rev.* **124**, 1866 (1961).  
<sup>4</sup> A.A. Clerk, X. Waital, and P.W. Brouwer, *Phys. Rev. Lett.* **86**, 4636 (2001).  
<sup>5</sup> K. Kobayashi, H. Aikawa, S. Katsumoto, and Y. Iye, *Phys. Rev. Lett.* **88**, 256806 (2002).  
<sup>6</sup> M.E. Torio, K. Hallberg, A.H. Ceccatto, and C.R. Proetto, *Phys. Rev. B* **65**, 085302 (2002).  
<sup>7</sup> T.F. Fang, W. Zuo, and J.Y. Chen, *Phys. Rev. B* **77**, 125136 (2008).  
<sup>8</sup> B.P. Buřka and P. Stefański, *Phys. Rev. Lett.* **86**, 5128 (2001).  
<sup>9</sup> K. Kang, S.Y. Cho, J.J. Kim, and S.C. Shin, *Phys. Rev. B* **63**, 113304 (2001).  
<sup>10</sup> M.E. Torio, K. Hallberg, S. Flach, A.E. Miroshnichenko, and M. Titov, *Eur. Phys. J. B* **37**, 399 (2004).  
<sup>11</sup> M. Lee and C. Bruder, *Phys. Rev. B* **73**, 085315 (2006).  
<sup>12</sup> J. Göres, D. Goldhaber-Gordon, S. Heemeyer, M.A. Kastner, H. Shtrikman, D. Mahalu, and U. Meirav, *Phys. Rev. B* **62**, 2188 (2000).  
<sup>13</sup> C. Morfonios, D. Buchholz, and P. Schmelcher, *Phys. Rev. B* **80**, 035301 (2009).  
<sup>14</sup> Z.Y. Zeng, F. Claro, and A. Pérez, *Phys. Rev. B* **65**, 085308 (2002).  
<sup>15</sup> R. Žitko, *Phys. Rev. B* **81**, 115316 (2010).  
<sup>16</sup> A.E. Miroshnichenko and Y.S. Kivshar, *Phys. Rev. E* **72**, 056611 (2005).  
<sup>17</sup> A. Chakrabarti, *Phys. Rev. B* **74**, 205315 (2006).  
<sup>18</sup> K. Kobayashi, H. Aikawa, A. Sano, S. Katsumoto, and Y. Iye, *Phys. Rev. B* **70**, 035319 (2004).  
<sup>19</sup> A.A. Aligia, and L.A. Salguero, *Phys. Rev. B* **70**, 075307 (2004).  
<sup>20</sup> R. Žitko and J. Bonča, *Phys. Rev. B* **73**, 035332 (2006).  
<sup>21</sup> B. Szafran and F.M. Peeters, *Phys. Rev. B* **72**, 165301 (2005).  
<sup>22</sup> B. Szafran and F.M. Peeters, *Europhys. Lett.* **70**, 810 (2005).  
<sup>23</sup> A. Fuhrer, S. Lüscher, T. Ihn, T. Heinzel, K. Ensslin, W. Wegscheider, and M. Bichler, *Nature (London)* **413**, 822 (2001).  
<sup>24</sup> U. F. Keyser, C. Fühner, S. Borck, R. J. Haug, M. Bichler, G. Abstreiter, and W. Wegscheider, *Phys. Rev. Lett.* **90**, 196601 (2003).  
<sup>25</sup> W. G. van der Wiel, Yu. V. Nazarov, S. De Franceschi, T. Fujisawa, J. M. Elzerman, E. W. G. M. Huizeling, S. Tarucha, and L. P. Kouwenhoven, *Phys. Rev. B*, **67** 033307 (2003).  
<sup>26</sup> A. Mühle, W. Wegscheider, and R. J. Haug, *Appl. Phys. Lett.* **91**, 133116 (2007).  
<sup>27</sup> F. Martins, B. Hackens, M.G. Pala, T. Ouisse, H. Sellier, X. Wallart, S. Bollaert, A. Cappy, J. Chevrier, V. Bayot, and S. Huant, *Phys. Rev. Lett.* **99**, 136807 (2007).  
<sup>28</sup> E. Strambini, V. Piazza, G. Biasiol, L. Sorba, and F. Beltram, *Phys. Rev. B* **79**, 195443 (2009).  
<sup>29</sup> E. Strambini, L. Chirolli, V. Giovannetti, F. Taddei, R. Fazio, V. Piazza, and F. Beltram, *Phys. Rev. Lett.* **104**, 170403 (2010).  
<sup>30</sup> L. Chirolli, E. Strambini, V. Giovannetti, F. Taddei, V. Piazza, R. Fazio, F. Beltram, and G. Burkard, arXiv:1004.1895v1.  
<sup>31</sup> P. Kwiat, H. Weinfurter, T. Herzog, A. Zeilinger, and M.A. Kasevich, *Phys. Rev. Lett.* **74**, 4763 (1995).  
<sup>32</sup> V.A. Mandelshtam, T.R. Ravuri, and H.S. Taylor, *Phys. Rev. Lett.* **70**, 1932 (1993).  
<sup>33</sup> M. Büttiker, *Phys. Rev. Lett.* **57**, 1761 (1986).  
<sup>34</sup> R. Akis, P. Vasilopoulos, and P. Debray, *Phys. Rev. B* **56**, 9594 (1997).  
<sup>35</sup> J.U. Nöckel, *Phys. Rev. B* **46**, 15348 (1992).  
<sup>36</sup> The barrier height  $V = 200$  meV is large as compared to the energy range of the lowest subband transport which for the system of Fig. 1 corresponds to the energy  $E$  lower than 4.5 meV. The wave functions vanish exponentially in the barriers with a penetration length equal to

$\hbar/\sqrt{2m^*(V-E)} \simeq \hbar/\sqrt{2m^*(V)}$ , which equals roughly 1.7 nm. This is small as compared to the width of the channels (64 nm). The effect of the finite barrier is an increased effective width of the channels. The bridge in the structure of Fig. 1 is necessary to allow the channel electrons to reach the ring.

<sup>37</sup> The finite difference approach naturally accounts for the evanescent modes [P.F. Bagwell, Phys.Rev. B **41**, 10 354 (1990)] which appear near the scattering region. The evanescent modes correspond to higher subbands and imaginary wave vectors (negative kinetic energy). They vanish exponentially away from the scattering point with a characteristic length equal to  $\lambda = \hbar/\sqrt{2m(E_n - E)}$ , where  $E_n$  is the threshold energy for the  $n$ -th subband. For the parameters considered in this paper the length is maximal in Fig. 6 (b) and equal to  $\lambda = 23$  nm which results from the second subband threshold  $E_n = 4.5$  meV and the considered energy  $E = 3.4$  meV. This length is small as

compared to the length of the computational box which covers 200 nm below and 200 nm above the contact to the ring. The evanescent modes do have influence on the  $c_{-k}$  and  $d_k$  values (reflected and transmitted amplitudes), but do not perturb their extraction from the finite difference wave function which is performed at the ends of the box of a proper size, where it takes the asymptotic form given by Eqs. (5) and (6).

<sup>38</sup> F.M. Peeters, in *Science and Engineering of One- and Zero-Dimensional Semiconductors*, edited by S.P. Beaumont and C.M. Sotomajor Torres (Plenum, New York, 1990), p. 107.

<sup>39</sup> M. Governale and C. Ungarelli, Phys. Rev. B **58**, 7816 (1998).

<sup>40</sup> L. Wendler, V.M. Fomin, and A.A. Krokhin, Phys. Rev. B **50**, 4642 (1994); L. Wendler, V.M. Fomin, A.V. Chaplik, and A.O. Govorov, Phys. Rev. B **54**, 4794 (1996).